MAUSAM, 48, 2 (April 1997), 123-134

551.515.2 : 551.551

Radial and vertical velocity field in a steady state symmetric tropical storm

J.C. MANDAL

Regional Meteorological Centre, Alipore, Calcutta, India

सार — चक्रवात के केन्द्र और उसके चारों ओर के ताप की विसंगतियों के कुछ ज्ञात मानों से स्थिर अवस्था अनुनादी उष्णकटिबंधीय चक्रवातों का अनुरूपी ढाँचा तैयार करने की एक विधि विकसित की गई है। उष्णकटिबंधीय चक्रवात में अनुप्रस्थ परिसंचरण उत्पन्न करने में विस्कासिता के गतिज भंवर के गुणांक के योगदान की जाँच की गयी है और उसकी चर्चा की गई है। उष्णकटिबंधीय चक्रवात के कुछ जाने-माने लक्षण और विशिष्टिताएँ, जैसे, चक्रवात की 'आई-वाल', आई-वाल की भीतरी अधोगामी गति, निम्न स्तरीय विकेन्द्रित अंतर्वाह और उच्च स्तरीय बहिर्वाह निदर्श में सही ढंग से व्यवस्थित किए गए हैं। गणना से यह पता चलता है कि भंवर के गुणांक के परिमाण की वृद्धि के साथ-साथ अनुप्रस्थ परिसंचरण में वृद्धि हुई है। परिसीमा स्तर में विकेन्द्रित भंवर के गुणांक की तुलना में उर्ध्वाधर भंवर के गुणांक का योगदान अधिक है, जबकि ऊपरी स्तर में पहले वाले गुणांक की तुलना में बाद वाला गुणांक अधिक महत्व रखता है। यह भी पाया गया है कि विकेन्द्रित एक्सचेंज गुणांक के नही होने पर चक्रवात के केन्द्रीय क्षेत्र में कोई अधोगामी गति की स्थिति नही हो सकती है। चक्रवात के 'आई' क्षेत्र में विकेन्द्रित और उर्ध्वाधर पवन का परिमाण विकेन्द्रित भँवर के गुणांक के परिवर्तन के प्रति अधिक संवेदी पाया गया है। भँवर के गुणांक के अतिरिक्त अनुप्रस्थ परिसंचरण भी परिसीमा स्तर के ऊपर स्पर्शी पवन के विस्तार पर निर्भर करता है।

ABSTRACT. A method to construct a consistent structure of steady state symmetric tropical storms from a few known values of temperature anomaly in the centre and around it has been developed. The role of kinematic eddy coefficient of viscosity in producing the transverse circulation in a tropical storm has been tested and discussed. The well known features and characteristics of a tropical storm, such as, eyewall, sinking motion inside the eyewall, low-level radial inflow and high level outflow are well produced in the model. The computation shows that there is an increase of transverse circulation with increase of the magnitude of eddy coefficient. In the boundary layer, the vertical eddy coefficient plays more important role than the radial eddy coefficient; while in the upper layer the latter is much more important than the former. It has also been found that in absence of radial exchange coefficient, there can be no sinking motion in the central region of the storm. The magnitude of radial and vertical wind in the eye region is more sensitive to the variation of radial eddy coefficient. In addition to the eddy coefficients, transverse circulations also depend upon the tangential wind distribution above the boundary layer.

Key words — Tropical storm, Eddy coefficients, Boundary layer, Radial, Vertical, Updraft, Tangential.

1. Introduction

Although the mean wind fields of tropical storms and their environment have received much attention, only the relatively dominant tangential flow is well documented. One of the most difficult variables to measure by direct means is vertical motion. It is generally agreed that out of the three wind components in a tropical storm, the tangential is best known, the radial is measurable but contains large errors, and the vertical is generally deduced from others. The case studies of individual storms using

conventional data do not provide sufficient accurate measurement of radial winds. Moreover, in data-sparse ocean areas, conventional observations are few and far between. Aircraft observations are the main source of data. But aircraft data received during storm periods have also been limited to a few levels per mission usually well below the maximum outflow level and above the boundary layer. This is also mainly confined to the inner storm region. Thus, none of the above data sources produces an accurate vertical profile of radial wind distributions. Without such a profile, it is difficult to compute other meaningful profiles of dynamic and thermo- dynamic variables, such as, energy, momentum, divergence or vertical velocity fields fully over the meso-scale storm area.

Few attempts have been made to obtain the vertical and radial velocity fields in tropical storms due to lack of data. Jordan (1952) and Hughes (1952) used composite data to analyse the upper and lower mean wind fields respectively around tropical storms. Miller (1958) updated these studied with an increased amount of data. All of these were done by hand computation using relatively small data set. The work of Palmen (1958), Palmen and Riehl (1957) and later work by Riehl and Malkus (1961) with aircraft reconnaissance data are early attempts to vertically integrate the horizontal divergence field and involve considerable skill. Krishnamurti (1961) pointed out that the above studies are concerned with a large scale and they do not give details of the vertical velocity field. He employed a more laborious method of characteristics in calculating vertical velocity from tangential velocity distribution at 15 km apart to a distance of 150 km from the centre and at 50 hPa intervals from 900 to 100 hPa obtained by interpolating available data around the centre of hurricane Cleo (1958) at flight levels 820, 580 and 237 hPa. He did not consider the boundary layer. The radial distribution of vertical velocity (or the stream function) at the top of the boundary layer controls the pattern of transverse circulation above the boundary layer including the outflow winds near the storm top. Barrientos (1964) computed radial and vertical velocity field in a steady state, circular symmetric hurricane from a given tangential wind field [same interpolated data of Cleo (1958) which were used by Krishnamurty (1961)] for various values of the exchange and drag coefficient. He considered the boundary layer as one layer and neglected the radial exchange coefficient in it. Shea and Gray (1973) computed structural variability of hurricane's inner core region from aircraft observational data. This study was confined on the flight data between 500 and 900 hPa levels. Tangential and radial winds were computed with reference to the radius of maximum wind. Using this data set, Gray and Shea (1973) computed vertical velocity and other dynamic and thermodynamic parameters. Frank (1977) made a composite study of ten years northwest Pacific rawinsonde data of 30 stations. He used these data to analyse large scale structure of tropical cyclones from 2-15° radius. Alongwith these data, he also used hurricane flight data composited by Shea and Gray (1973) to analyse the inner spiral bands, eye and eyewall region (0-2°). The most part of this study was confined with mean steady state typhoon data.

Though research aircraft missions and synoptic data have demonstrated important asymmetries and meso-structural details of a tropical storm, the symmetric model remains attractive because of it's simplicity and because the extent to which tropical storm structure can be computed with this model has not been ascertained.

A real tropical storm may be in a steady state for only a short time, and may never be perfectly symmetric. However, it is probable that a major part of the storm's dynamics can be accounted for by the steady symmetric approximation.

Riehl (1963) performed several simple integration using aircraft data of six hurricanes to determine what extent a steady hurricane model can be used to approximate observed storm structures. He concludes that the crude model for symmetric vortex calculations are useful for describing some important structural features of several hurricanes, especially the more intense ones.

Radial motion and, hence divergence and vertical motion, in a steady state symmetric vortex can exist only in the presence of tangential friction. The field of vertical motion in a storm must, therefore, be closely related to the frictional force field.

One of the main objectives of this work is to describe in quantitative terms some features of tropical storm circulations observed in a large fraction of cases using tangential velocity, pressure and temperature distribution above the boundary layer by the method of Mandal (1988) (hereafter called paper I), and within the boundary layer solutions by the method in Mandal (1992) (hereafter called, paper-II). Our

procedure for calculation is similar to one followed by Barrietos (1964). More significantly, the present model considers the boundary layer as 40-layer instead of one layer, and the upper region is divided into 91 divisions.

2. Numerical procedure

A cylindrical coordinate system is employed with height, z as vertical coordinate positive upwards, the azimuth angle θ is positive in the counter clockwise direction and the radial coordinate, r is increasing outward (positive) from the storm's centre, which is the origin.

The vortex will be assumed (*i*) to be in a steady state which eliminates the local time derivative and reduces the equation to a diagnostic form, and, secondly, (*ii*) all variables will be assumed axially symmetric which reduced the problem to two dimensions.

The following three steps are followed to obtain the solution :

(a) *Step-I : Tangential velocity and pressure fields above the boundary layer*

Knowing the maximum temperature anomaly in the centre and at a few points around it in the upper layer, and an approximate radius of inner eyewall cloud from satellite imagery the temperature distribution on any vertical plane through the centre of the storm is calculated (paper-I). From this, the tangential velocity and pressure field distribution on the same plane is calculated assuming gradient wind balance following the procedure laid down in the same work. The computations have been made taking 200 grid point in the vertical direction.

(b) *Step-II : Tangential, radial and vertical wind and stream function distribution in the boundary layer*

The tangential wind profile above the boundary layer obtained in the Step-I is superimposed on the boundary layer. The solutions for the above variables in the boundary layer are computed following the procedure devised in paper-II. Assumptions, scaling factors etc. are same as in that work. Here, the vertical grid length is 40 m, and that in radial direction is 1.25 km in the central region and thereafter increased step by step.

(c) *Step-III : Transverse circulation above the boundary layer*

To get the tangential velocity and pressure distribution on r-z plane above the boundary layer, the radial equation of motion and hydrostatic equation have been used, under these assumptions the remaining equations of motion for turbulent flow in a rotating frame of reference with variable eddy coefficient of viscosity (*i.e.*, exchange coefficients) can be put in the following form:

$$u\frac{\partial v}{\partial r}+\frac{uv}{r}+w\frac{\partial v}{\partial z}+fu=\frac{\partial}{\partial r}\left[K_r\left(\frac{\partial v}{\partial r}+\frac{v}{r}\right)\right]+\frac{1}{\rho}\frac{\partial}{\partial z}\left[\rho K_z\left(\frac{\partial v}{\partial z}\right)\right] \quad (1)$$

The equation of continuity is,

$$\frac{\partial}{\partial r}(\rho ur)+\frac{\partial}{\partial z}(\rho wr)=0 \quad (2)$$

and the equation of state is given below :

$$p=\rho RT \quad (3)$$

where, v is the tangential velocity, positive in the counter clockwise direction; u is the radial velocity, positive outwards; w is the vertical velocity, positive upward, ρ is density; T is air temperature; R is specific gas constant; 'f' is Coriolis parameter; K_r and K_z are respectively the radial and vertical kinematic eddy coefficient of viscosity. (It may be mentioned here that energy equation is not required as a temperature field has been defined). The form of the Eqn. (1) is similar to one used by Rosenthal (1969) in his multilevel primitive equation model to simulate the development of a tropical cyclone.

The Stoke's stream function ψ, which satisfies, the continuity Eqn. (2) is defined by:

$$\rho ur=\frac{\partial\psi}{\partial z};\quad \rho wr=-\frac{\partial\psi}{\partial r} \quad (4)$$

Representing the absolute angular momentum, $(vr+\frac{1}{2}fr^2)$ per unit mass about the vertical axis at the centre of the storm by ϕ, the following relations are obtained:

$$\frac{\partial\phi}{\partial r}=r\left(\frac{\partial v}{\partial r}+\frac{v}{r}+f\right)$$

$$\frac{\partial \phi}{\partial z} = r \frac{\partial v}{\partial z} \qquad (6)$$

Substituting Eqns. (4), (5) and (6) into Eqn. (1) and rearranging terms we get:

$$\frac{\partial \phi}{\partial r}\frac{\partial \psi}{\partial z} - \frac{\partial \phi}{\partial z}\frac{\partial \psi}{\partial r}$$

$$= r^2 \rho \frac{\partial}{\partial r}\left[K_r \left(\frac{\partial v}{\partial r} + \frac{v}{r} \right) \right] + r^2 \frac{\partial}{\partial z}\left[\rho K_z \left(\frac{\partial v}{\partial z} \right) \right] \qquad (7)$$

For any prescribed field of tangential velocity, v Eqn. (7) is a first order linear differential equation in ψ, so boundary conditions are required for each of the independent variables, r, and z.

Boundary conditions

(1) The stream function on the axis of the model ($r = 0$) is assumed to be zero. This is consistent with the symmetry assumption.

(2) The values of the stream function at the top of the boundary layer along radial distance, r are taken from computation made in Step-II.

If the kinematic eddy coefficients, the tangential velocity field, temperature and pressure (hence, density, ρ) on r-z plane are known, Eqn. (7) can be solved for the stream function ψ. After evaluation of the stream function, radial and vertical velocities can also be computed from Eqn. (4).

3. Computational method

All computations are done using a finite difference approximation for the differential equation. An interlacing frid system (not shown) is used to provide maximum resolution by permitting derivatives to be approximated by difference over one grid length rather than two. The main grid consists of 51 points in the vertical and 81 points in the radial direction. The intermediate grid is placed in between the main grid points. The stream function, ψ is defined on the main grid points. As v, p and T can be calculated at as many points as desired, these variables are defined both on the main grid and intermediate grid points as well as on the crossing points of the two grids. Eddy coefficients of viscosity K_r, and K_z are defined on the main grid. This arrangement improves the accuracy of the finite difference scheme.

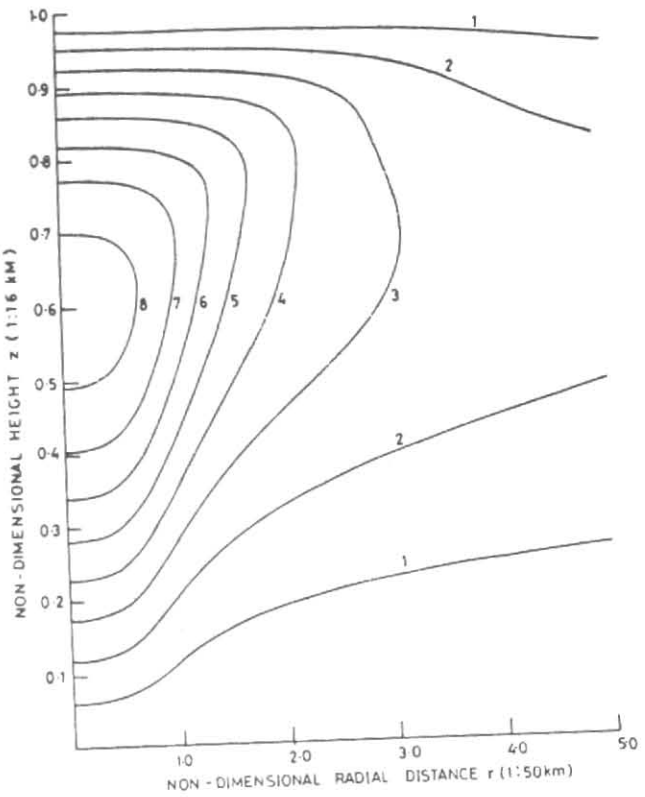

Fig. 1. Vertical cross-section of temperature anomaly (°C)

A finite difference equation corresponding to the Eqn. (7) can be written as:

$$\delta r\phi \cdot \overline{\delta_z \psi^r} - \delta z\phi \cdot \overline{\delta_r \psi^z} = \overline{S}\,(r, z) \qquad (8)$$

where $\overline{\delta_z \psi^r}$ implies averaging along r after taking derivative along z. Other symbols have similar meaning.

The tangential velocity, pressure and temperature data are used as input from Step-I. The density, ρ is calculated using equation of state (3). The term $\overline{S(r, z)}$ containing the radial and vertical exchange co-efficient is defined at the intermediate grid point which is consistent with the averaging scheme. Scaling of the thermodynamic variables is made as in work of Step-I, and other variables as in work in Step-II. Thus, Z_0 is 1 km and r_0 is 50 km.

As the stream function is known on the axis (as a boundary condition) and at the top of the boundary layer (computed from Step-II, the stream

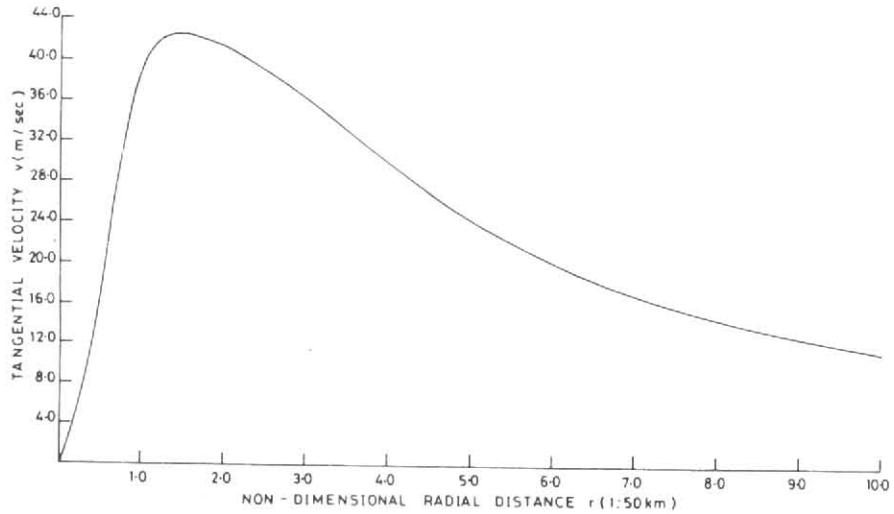

Fig. 2. Tangential velocity profile super-imposed on boundary layer (m/sec)

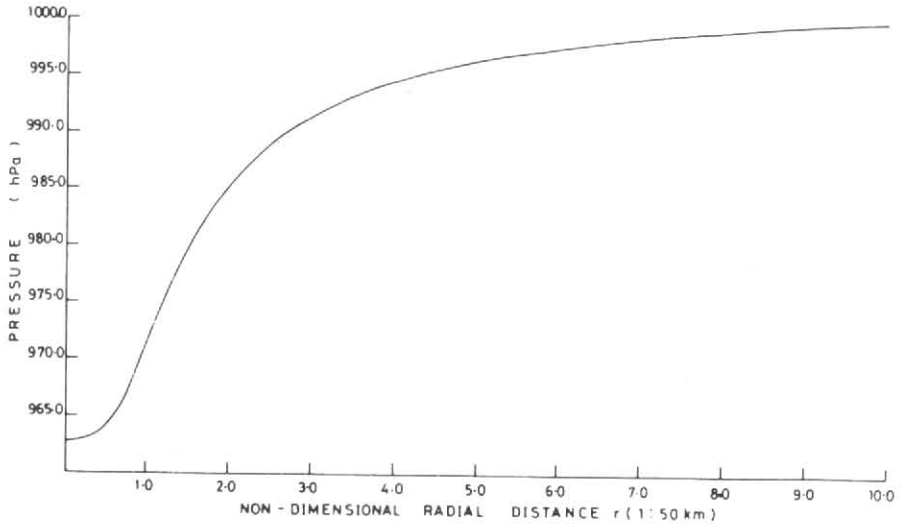

Fig. 3. Surface pressure profile (hPa)

function at $r = \Delta r$ and $z = \Delta z$ can be computed from:

$$\Psi_{i+1,j+1} = [2 \cdot \Delta r \cdot \Delta z \cdot \bar{S}(r, z)_{i,j} - \delta_r \phi_{i,j} (\Psi_{i+1,j} - \Psi_{i,j} - \Psi_{i,j+1}) \Delta r + \delta_z \phi_{i,j} (\Psi_{i,j+1} - \Psi_{i,j} - \Psi_{i+1,j}) \Delta z] / [\Delta r \, \delta r \phi_{i,j} - \delta z \phi_{i,j} \Delta z] \quad (9)$$

where i (=1, ... M), and j (=1, ... N) are the indices in the vertical and radial directions respectively. Computations can be made either along r or z. Computations of the other parameters can be done as previously outlined. It was observed that there is no difference in results whether the computation is started from left to right or from bottom to top of the upper layer.

3.1. *Input data fields*

Temperature excess to the tune of 15°C has been observed at 250 hPa from the reconnaissance data in some intense storms (Gray and Shea 1973). For this study, a moderate storm has been considered, so the maximum temperature anomaly of 8.5°C has been put. The resulting temperature anomaly distribution on the radial axial plane is shown in Fig. 1. It is a typical distribution. The radial gradient of temperature anomaly (hence, of temperature) is very weak in the centre, gradually increases with radial distance and reaches a maximum near the eyewall region and then decreases outward. Resulting radial profile of surface tangential velocity, v is shown in

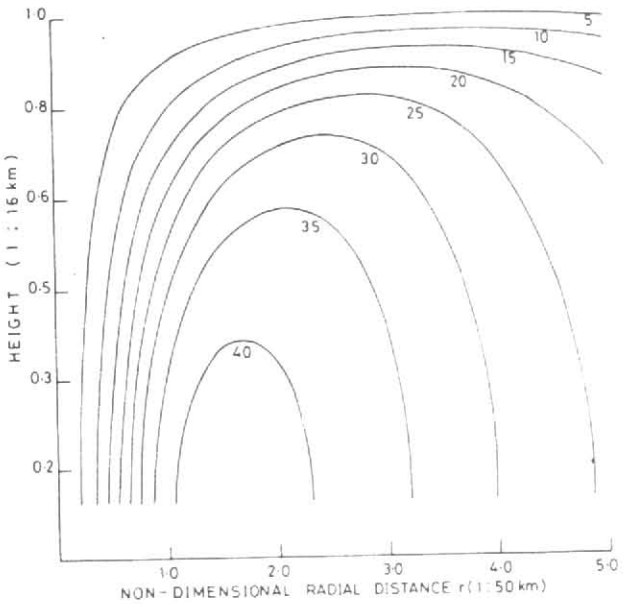

Fig. 4. Vertical cross-section of tangential velocity (m/sec)

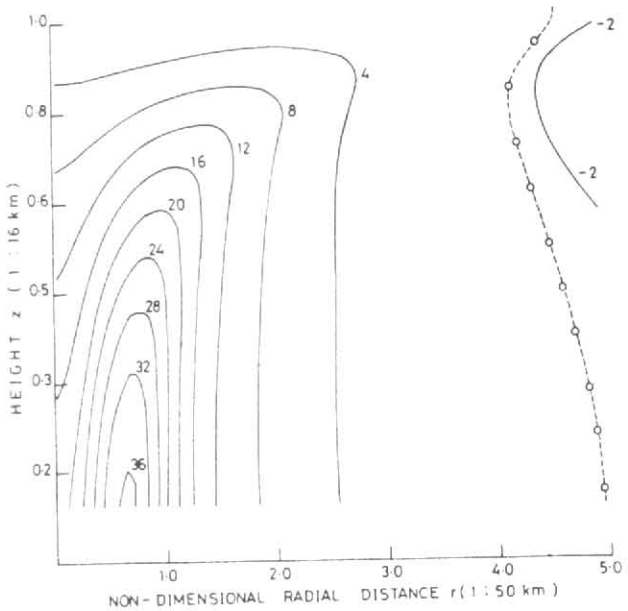

Fig. 5. Vertical cross-section of relative velocity, ζ ($5\times\ 10^{-5}$ sec^{-1})

Fig. 2. As expected, initially in the centre, increase of v with r is very small. It's rate of increase with r gradually increases, becomes maximum before the maximum value of 42.5 m/s is reached nearly at r = 1.45, then decreases slowly with r. It exhibits a smooth peak at the radius of maximum wind (RMW) and shows anticyclonic shears outside the RMW, though not very steep. The pressure profile on the sea surface is shown in Fig. 3. It clearly shows that the pressure gradient is highest in the eyewall region and very small near the centre. The vertical cross section of tangential velocity is shown in Fig. 4. The flow decreases in intensity with increasing radius from RMW and increasing height. The radius of maximum wind increases with height. In the lower troposphere, vertical wind shears are quite weak. The pattern is similar to one presented by Krishnamurty (1961) from data of hurricane Cleo (1958) and many other individual case studies. The vertical cross-section of relative vorticity is shown in Fig. 5. The concentration of vorticity just inside the radius of maximum wind is due to very large horizontal wind shear is readily seen. It reflects the basic character of the sharply peaked wind speed profile. Near the eyewall region, its maximum value approaches to 183×10^{-5} sec^{-1}, a moderate value. At about 50 km from the RMW, it has dropped to nearly 20.0×10^{-5} sec^{-1}. The maximum value of vorticity tilts outward with height as does the maximum winds in the eye wall. The vertical cross-section of absolute angular momentum is shown in Fig. 6. At 200 km from the centre it is more than 320×10^5 m^2 sec^{-1}, while around the eyewall it is only $20 - 50 \times 10^5$ m^2/sec, about one order of magnitude smaller than the former. This figure reveals a reasonable distribution of the angular momentum in the radial-vertical plane. This figure also shows that the inward moving air in the inflow layer lost momentum to the sea at an increasing rate. Below 5 km, the values are nearly constant with height. If we assume that this space cross-section represents the case of steady state tropical storm and that the absolute angular momentum is conserved through outflow processes, except near the surface, the iso-lines of the absolute angular momentum would represent stream line in a radial-vertical plane.

4. Numerical experiments

It has been mentioned that the computed flow pattern above the boundary layer as shown by the stream function from which the radial and vertical velocity can be calculated, depends upon the following four sets of given conditions, namely, (a) the boundary conditions and modeling approximation used, (b) the tangential wind distribution above the boundary layer, (c) the stream function at the top of the boundary layer, and finally (d) spatial distribution of eddy coefficient of viscosity.

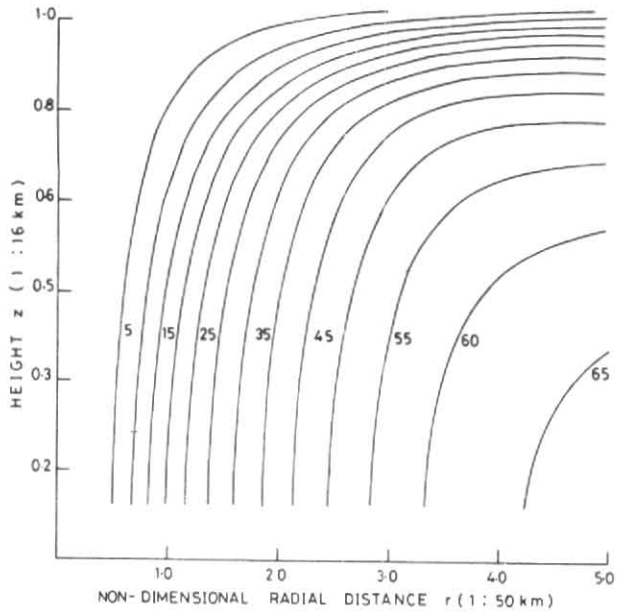

Fig. 6. Vertical cross-section of absolute angular momentum (5×10^5 m^2/sec)

For the modelling approximation, we have used very fine resolution taking 160 m grid length in the vertical direction, and upto 150 km from the centre of the storm, the radial grid length is 1.25 km, thereafter it is increased gradually step by step. To calculate the boundary layer variables, the grid length both in the radial and vertical (40 m) directions are also very fine. The approximation made in the Navier-Stoke's equation of motion is the hydrostatic assumption in the third equation of motion and gradient wind balance in calculating the tangential wind distribution in Step-I. These approximations are justified by scale analysis (vide, paper-I).

For the present work, mainly one set of tangential velocity field distribution would be considered for detail computation. In future works, rigorous study is contemplated to be made varying the distribution of this field.

The conditions in the surface boundary layer (friction layer) are critical for the resulting flow pattern. Several major characteristics of the transverse circulations are changed appreciably by slight variation in the boundary layer parameters. As this work is the continuation of previous two works, we will restrict our computation with the variation of vertical eddy coefficient of viscosity, K_z for which we got best results, namely, we will take K_z, proportional to the radial variation of superimposed tangential velocity profile at the top of the boundary layer. Here, we will include radial coefficient, K_r with constant value throughout the boundary layer. The boundary layer in this chapter refers to the layer from the surface to the bottom of the upper layer, *i.e.*, upto 1.6 km. Strictly speaking, the whole layer is not the boundary layer since the depth of the boundary layer in a tropical storm is not constant radially. It has been shown in the work of paper-II, that the boundary layer thickness decreases sharply from the radius of maximum tangential velocity to the centre of the storm. As computations for all variables in this layer are made upto this height and also to avoid irregular grid, the computation for the upper layer would be made from this height. In our discussion, the surface inflow layer will refer to the layer from the sea surface to the level from where radial velocity changes from inflow to outflow.

In as much as one of the main purposes of this work is to determine reasonable values of the eddy coefficient, several sets of experiments were performed for the upper layer on the same input data. Horizontal and vertical eddy coefficients were varied systematically based on the present limited knowledge about them for different sets of experiments. The results of the experiments were analysed and the relevant ones are discussed in this section to illustrate the more pertinent ones.

It has already been pointed that there is no unique method to determine the space variation of kinematic eddy coefficient of viscosity. Regarding the influence of vertical eddy coefficient in the boundary layer, discussions have been made in paper-II. In numerical models, researchers generally choose constant values for radial (horizontal) eddy coefficient, K_r. Its value in most studies lies in the range from 10^3 to 5×10^4 m^2/sec; some even take a value as high as 2.7×10^5 m^2/sec.

Anthes *et al.*, (1971) pointed out that preliminary tests as well as calculation with a symmetrical model revealed that neither a constant value of K_r, nor a variable K_z proportional to the magnitude of the total deformation of the horizontal motion provide acceptable results, and ultimately they put $K_r = 10^3 \text{ m } | V | + 5 \times 10^3$ m^2/sec. They further argue that though this was not very satisfactory from physical point of view, it did afford a usual representation of the statistical effect of horizontal interaction between momentum fields of the cumuli and meso-scale.

As the vorticity field is one of the significant properties of the tangential velocity distribution of tropical storms, and vertical motion is related to it, we have associated this field with radial eddy coefficient, K_r. Evidently, more satisfactory formulations are dependent on the success of the theoretical and observational interaction. Thus, in our numerical experiments, in the boundary layer, as well as in the upper layer we would take $K_z = 50\ (v/v_{max})m^2/sec$, as it was found more suitable in the paper-II. In addition to this we would include radial coefficient, K_r in the boundary layer. For simplicity, constant values of K_r would be considered in the boundary layer. In the upper layer, values of K_r are taken in the following form:

(*i*) Case (A) : $K_r = c_1$

(*ii*) Case (B) : $K_r = c_1 + c_2 | v |$

(*iii*) Case (C) : $K_r = c_4 + c_5 | \partial v/\partial r + v/r |$

where v and $(\partial v/\partial r + v/r)$ are nondimensional tangential wind and absolute value of relative vorticity; dimension of c_1, c_2, c_3, c_4 and c_5 is m^2/sec.

The appropriate values of these parameters would be mentioned during discussions.

4.1. *Results from numerical experiments*

From the results of the numerical experiments, it has been observed that if the radial gradient of vorticity in superimposed tangential wind profile is small, there is practically no change in the boundary layer flow, whether K_r is included or not. But, if the gradient of vorticity is not insignificant, with inclusion of K_r, the value of maximum upward velocity at the top of the boundary layer increases and near the centre, its magnitude decreases. In the present experiments when K_r was taken $10^4 m^2/sec$, even downward motion appeared in the boundary layer (within 1.6 km) near the centre.

Numerical computations have been done varying K_r from 5×10^3 to $10^4 m^2/sec$ in the boundary layer and by taking a constant $K_r = 2.5 \times 10^4 m^2/sec$ in the upper layer. It is noticed that with increasing K_r in the boundary layer and keeping the same constant value in the upper layer, the maximum value of both upward and downward velocity near the centre increases, and the vertical location of the maximum values of both come down. Sinking motion in the centre also comes closer to the surface. The maximum outflow in the upper troposphere and inflow in the upper part of the eye increase slightly.

If in the boundary layer K_r is taken as zero, or $\leq 5 \times 10^3\ m^2/sec$ and in the upper layer K_r is also zero, no sinking motion is observed in the eye. However, if K_r in the boundary layer is increased to $10^4 m^2/sec$, light sinking motion of – 6.24 cm/sec appears in the centre; very weak inflow in the upper part of the eye also appears. There is no change in the flow pattern in the upper layer, whether K_z is included or not, only the magnitude of radial and vertical velocity increases slightly.

Keeping the same value of K_r in the upper layer, if the value of K_r in the boundary is increased, then with increase of the strength of transverse circulation in the boundary layer, the strength of transverse circulation in the upper layer also increases. If both in the boundary layer and upper layer K_r is kept zero, neither the sinking motion in the centre, nor the inflow in the upper part near the centre is observed; everywhere above the surface inflow layer, the motion is upward and outward.

The general result of computation is an increase of the transverse circulation with increasing values of the eddy coefficients. In the boundary layer, the vertical eddy coefficient plays more important role than the radial coefficient; while in the upper layer the latter is much more significant than the former. The pattern of transverse circulation is mainly dependent upon the tangential velocity distribution. The magnitude of radial and vertical wind components in the eye is more sensitive to the variation of K_r.

Above discussions prove that boundary layer mechanism has a great influence on the transverse circulation in the upper layer also.

Fig. 7 shows the vertical cross section of the Stoke's stream function of the flow obtained by taking $K_r = 0$ in the boundary layer, and both K_r and K_z to zero in the upper layer. This can be considered as an extreme case. This simulates the condition that there is no radial friction in the boundary layer and internal friction in the upper layer. The circulation might be

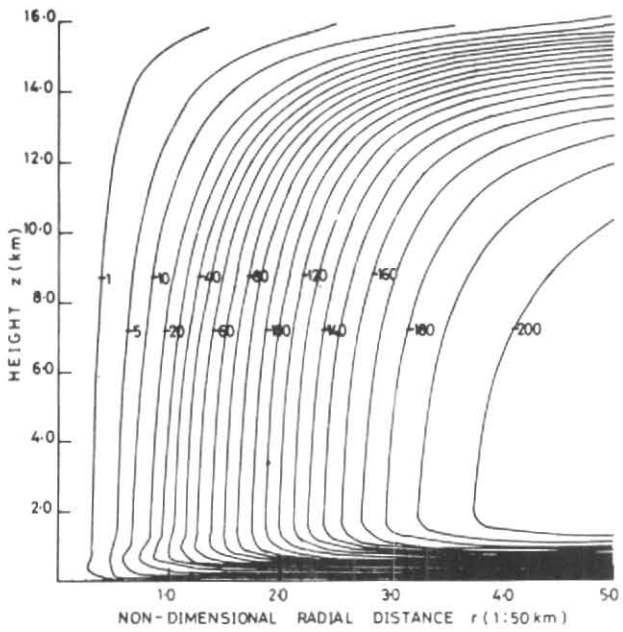

Fig. 7. Stream function, ψ (10^7 kg/sec), in boundary layer : $K_z = 50\ \nu\ /\nu_{max}$ and in upper layer : K_z , $K_r = 0$

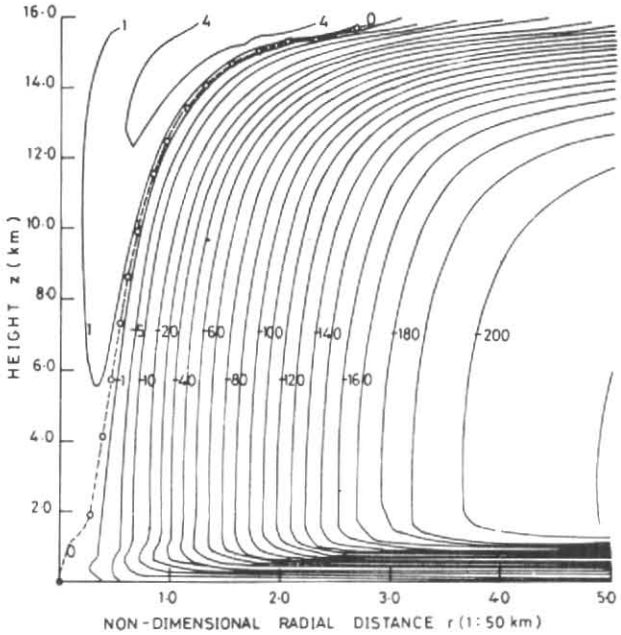

Fig. 8. Stream function, ψ (10^7 kg/sec), Case (C): $K_z = 50\ \nu/\nu_{max}$; $K_r = 10^4$ (1.5 + 0.1 × non-dim ζ) in m^2/sec

obtained only to the exchange of vertical eddy momentum flux in the boundary layer. As expected, the flow above the boundary layer is mainly upward and outward. The conditions also imply that the inflow is confined mainly to the boundary layer which is evident from the figure. It may be noted that the region of maximum upward vertical velocity is controlled by the region of maximum upward velocity at the top of the boundary layer.

Computations have been carried with different values for c_1, *i.e.*, constant K_r, and different combinations for c_2 & c_3 and c_4 & c_5. For the tested three cases, if the following values for K_r, *viz.*

(*i*) Case (A) : $K_r = 5 \times 10^4 m^2/sec$,

(*ii*) Case (B) : $K_r = 1.5 \times 10^4 m^2/sec + | v |$ $2.5 \times 10^3\ m^2/\ sec$

(*iii*) Case (C) : $K_r = 1.5 \times 10^4\ m^2/sec + | \partial v/\partial r + v/r | \times 10^3\ m^2/sec$

are taken, all cases can reproduce the important characteristic features in the central eye region with comparable values of the sinking motion inside the eye wall, rising motion in the eye wall and inflow in the upper part of the eye. But, the weak inflow or outflow in the middle troposphere in outer region and depth of inflow in the upper part of the eye are different. The depth of inflow in the upper part of the eye is highest in case C and lowest in case A, and case B is in between them. In case B, the height of the inflow in the outer region extends upto 9.2 km, while in case A, upto 5.6 km and upto 2.2 km in case C. In all cases strong outflow is confined in the upper troposphere.

The field of stream function in case (C) is presented in Fig. 8. The eye wall is represented by the zero line (broken) of stream function that divides the region of upward and downward motion. The computed transverse circulation indicates strong inflow in the boundary layer and strong outflow near the top of the upper layer. If approached from outer region, initially the depth of the inflow layer decreases slowly, but near the RMW, it decreases very sharply. In the centre near the surface, outflow is also evident from the stream line pattern. The well known features of tropical storms, such as the eye, the eye wall and the high level outflow is clearly illustrated in the figure.

The vertical cross section of radial velocity in case (C) is shown in Fig. 9. There is a deep and narrow inflow layer on the top near the centre which is accompanied by sinking motion in the eye. The maximum outflow in the upper troposphere in this

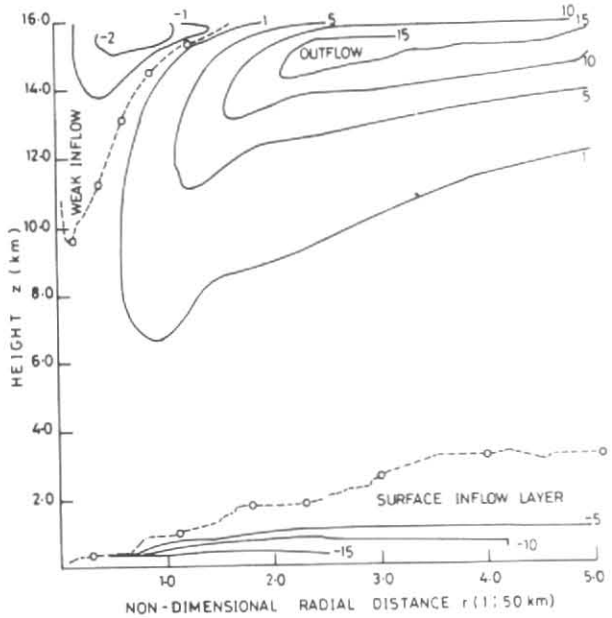

Fig. 9. Radial velocity, u (m/sec), Case (C): $K_z = 50\ v/v_{max}$; $K_r = 10^4$ (1.5 + 0.1 × non-dim ζ) in m^2/sec

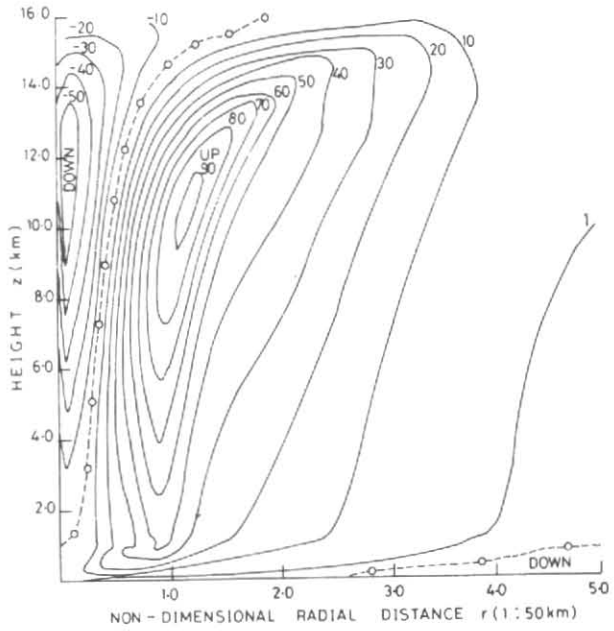

Fig. 10. Vertical velocity, w (cm/sec), Case (C): $K_z = 50\ v/v_{max}$; $K_r = 10^4$ (1.5 + 0.1 × non-dim ζ) in m^2/sec

case is 22.8 m/sec at radial distance, r = 3.5 (175km) and those in cases (A) and (B) are 24.6 m/sec at r = 3.7, and 22.9 m/sec at r = 3.2 respectively (Figs. not shown). The maximum inflow at the upper troposphere inside the eye wall in cases (A), (B) and (C) are – 3.12 m/sec at r = 0.70, – 2.18 m/sec at r = 0.35 and – 2.75 m/sec at r = 0.80 respectively. In all cases the height of maximum inflow or outflow is at 15.5 km, i.e., only 0.5 km below the top of the grid considered. The radial distance of maximum upper tropospheric outflow is much away from the RMW at the surface. But, as the radius of maximum tangential wind slopes outward with height, it is near the maximum wind at that level. The magnitude of maximum outflow appears higher in comparison with that in the models of Krishnamurty (1961) and Barrientos (1964). In case studies, data at such height are hardly available. Keeping the same maximum tangential wind speed, and increasing the rate of decrease of speed outside the radius of maximum wind, numerical experiments were also performed, and it was revealed that the magnitude of outflow (with that distribution of tangential wind field) decreases. It was also noticed that the radial extent of strong upward motion shrinks due to decrease of radial extent of strong inflow (hence, total inflow) in the boundary layer. Thus, it is confirmed as suggested by the mass continuity equation that the magnitude of outflow depends upon the updraft which again depends upon the tangential wind profile at the top of the boundary layer and boundary layer mechanism.

The surface boundary layer exhibits inflow from the outer region to the area of RMW. The magnitude of this inflow is highest at a distance from the RMW and decreases sharply as RMW is approached and outflow appears near the centre. This is also supported by the stream line pattern in Fig. 8. The 1 m/sec isoline of u sloped down to the eye wall region. Above the boundary layer the radial flow, whether it is inflow or outflow, is very weak up to the lower part of the upper troposphere in all cases. Gray and Shea (1973) in their study with composite data have found strong convergence in the lowest layer at and outside the radius of maximum winds but approximately just within the surface friction boundary layer. By contrast, middle levels show very little over all inflow or outflow around the RMW.

In case (C), the surface inflow layer is confined within 1.6 km upto radial distance r = 2.6 (130 km), then gradually increases (Fig. 9) to a variable height, but not more than 3.2 km; while in cases (A) and (B), (Figs. not shown) the inflow extends

above 1.6 km much earlier, and at r = 4.4 (220 km), it extends even upto 9.4 km (which appears not to be realistic), then becomes irregular.

The vertical cross section of vertical motion in case (C) is shown in Fig. 10. The profile of vertical velocity exhibits all important characteristics of tropical storm. The zero line of vertical velocity may be considered as the inner boundary of the eye wall. A strong upward motion is seen at the eye wall and sinking motion in the eye. It may be seen that the eye wall slopes outward with height. The upward motion at twice the radius of RMW is an order of magnitude lower than that at the eye wall. The region of maximum upward motion in this study lies inside and closed to the maximum tangential wind speed which agree with the studies of Gray and Shea (1973), Krishnamurty (1961) and Barrientos (1964).

The maximum upward motion in case (C), is 92.4 cm/sec (Fig. 10) at r = 1.175 (58.75 km) and at height, 10.88 km and maximum sinking motion inside the eye wall region is – 58.3 cm/sec, while those in case (A) are 91.6 cm/sec (r = 1.275, z = 11.2 km) & – 70.3 cm/sec (r = 0.075, z = 11.52) and in (B) 97.8 cm/sec (r = 1.325, z = 11.20) & –56.1 cm/sec (r = 0.075, z = 12.8 km) respectively. In all cases, radial position of maximum upward velocity is inside the radius of maximum tangential velocity and slopes outwards with height. The vertical position of maximum upward velocity is lowest in case (C) which seems to be more realistic than other two cases.

Gray and Shea (1973) calculated kinematically the vertical velocity in the inner core region of mean tropical storm (v_{max} = 90 kt ≈ 45.7 m/sec). They mentioned that the largest ascending vertical motion (~ 5000 hPa /day ≈ 80 cm/sec) were concentrated in a narrow area around the radius of the maximum wind. They also found a narrow region of strong subsidence (~ 4000 - 5000 hPa/day) approximately 5-7 nautical mile inside the RMW and well inside the RMW weaker subsidence was present. They also pointed out that although mean ascending vertical motion within the eye wall clouds of approximately 80 cm/sec appear to be low for hurricane; case studies indicate that the hurricane does not have uniform vertical motion pattern. Only a small portion of the inner core area is covered by strong updrafts. Assuming that 10% of the eye wall region is covered by intense convection mean middle level ascending vertical motion of about 8 m/sec would be present in this region.

Bergman and Carlson (1975) have developed a method for objective analysis of aircraft observations in tropical storms. The aircraft flew a series of 10 passes through the eye of the storm, Debbie (August 1969) at about 3.5 km (650 hPa). According to them tangential wind and vertical motions have an almost circularly symmetric distribution but with slightly higher speed in the southern quadrant. The tangential wind at this level was 45 m/sec (at the surface it would be more); maximum upward vertical velocities in the eye wall are only slightly more than 1 m/sec, but there is evidence of substantial descending motion in the eye. At the same level in hurricane Ginger (September 1971), the maximum wind speed was slightly more than 30 m/sec, and maximum updraft of 70 cm/sec with highest downdraft of 50 cm/sec was observed.

In his computation with interpolated data of Cleo (1958) (v_{max} = 65 kt ≈ 33 m/sec) Krishnamurty (1961) got maximum updraft in the eye wall and downdraft in the eye of the order of –250 and 200 hPa /hr respectively. He took $K_r = 2.7 \times 10^5$ m^2/sec, which appears to be very high. With same data set, and $K_r = 3 \times 10^4$ m^2/sec, Barrientos (1964) got maximum updraft and downdraft in the same regions slightly more than – 100 and 100 hPa /hr respectively. It is most likely that in real storm the maximum updraft in the eye wall is greater than the maximum downdraft in the eye.

In tropical storms, systematic vertical velocity profiles become evident when the small-scale fluctuations are eliminated by smoothing and compositing of the data. The cumulus updraft and downdrafts appear to be superimposed upon a large band scale of motion that is more stable and coherent in time than the individual cloud features.

From the above discussions, it appears that the magnitude and positions of maximum radial and vertical wind speed in case (C) of this model are well within reasonable limits. In addition to the eddy coefficients, they are dependent upon the superimposed (*i.e.* just at the top of the boundary layer) tangential wind profile and also tangential wind distribution in the upper layer.

5. Conclusion and remarks

In this study we have obtained the structure of a steady state symmetric tropical storm for a prescribed tangential wind velocity field which has been determined from temperature anomaly distribution. The well known features and characteristics of a tropical storm, such

as, the eyewall, sinking motion inside the eyewall, the low-level radial inflow, high-level outflow are well reproduced in the model. Within the frame work of the model, the transverse circulation of a tropical storm depends upon the tangential velocity distribution, mechanism in the boundary layer and exchange process within the storm. The internal friction (turbulent mixing) in the fluid represented by the eddy coefficient affects the flow considerably. In the boundary layer, the vertical eddy coefficient plays more important role than the radial exchange coefficient; while in the upper layer the latter is much more significant than the former. It has also been seen that in absence of radial eddy coefficient above the boundary layer, there can be no sinking motion in the central region of a tropical storm. With the increase of the value of this coefficient, both the radial and vertical velocity increase in magnitude, though the pattern remains the same. After consideration of several factors, it may be concluded that the following values seem to be more appropriate for the tropical storm: (a) in the boundary layer $K_r = 10^4$ m^2/sec; $K_z = 50$ m^2/sec (v/v_{max}) and (b) in upper layer, K_r = (1.0 to 2.0) 10^4 m^2/sec + $|\partial v/\partial r + v/r| \times$ (1 to 1.5) $\times 10^3$ m^2/sec. However, these magnitudes can not be taken literally, as the values for a storm. In the initial stage, the magnitude may be less than these values. Further experiments on a similar line should be carried out to understand the space variation of K_r and K_z. Comparison can be made with more confidence, if alongwith tangential wind, radial wind component can be measured from real storms with sufficient accuracy.

The results do appear to have sufficient accuracy to permit use in many diagnostic studies. They would provide a useful set of analysis for comparison with numerical models which simulate the structure and dynamics of tropical storms. Moreover, these results can be generated at a modest expense and in a very relatively short time once the aircraft or dropsonde data for temperatures have undergone their initial processing. More detailed analyses of selected areas of a tropical storm may be produced by reducing the grid spacing.

One of the drawbacks of the model is that it could not reproduce sinking motion just outside the eye wall region. This type of sinking motion may be the effect of thermodynamic and other dynamic conditions. To a great extent, tangential wind field distribution may be responsible for it.

Acknowledgements

The author expresses his deep sense of gratitude to Dr. M.K. Guha, Dy Director General of Meteorology, RMC, Calcutta, for his encouragement, and computer and other facilities provided for this work. He is also thankful to all members of staff in Computer Unit of R.M.C., Calcutta for their co-operation and help during this work.

References

Anthes, R.A., Rosenthal, S. L. and Trout, J. W., 1971, "Preliminary results from an asymmetric model of tropical cyclone," *Mon. Wea. Rev.*, 99, 744-758.

Barrientos, C.S., 1964, "Computation of transverse circulation in a steady state symmetric hurricane," *J. Appl. Meteor.*, **3**, pp. 685-692.

Bergman, K. H. and Carlson, T. N., 1975, "Objective analysis of aircraft data in tropical cyclones," *Mon. Wea. Rev.*, **103**, pp. 431-444.

Frank, W.M., 1977, "The structure and energetics of the tropical cyclone, I-storm structure," *Mon. Wea. Rev.*, **105**, 1119- 1135.

Gray, W. M. and Shea D. J., 1973, "The hurricane inner core region II. Dynamic and thermodynamic characteristics," *J. Atmos. Sci.*, **30**, 1565-1576.

Hughes, L. A., 1952, "On the low level wind structure of tropical cyclones", *J. Meteor.*, **9**, 442-448.

Jordan, E. S., 1952, "An observational study of the upper wind circulation around tropical storms", *J. Meteor.*, **9**, 340- 346.

Krishnamurti, T. N., 1961, "On the vertical velocity field in a steady symmetric hurricane," *Tellus*, **XIII**, **2**, 171-180.

Mandal, J. C., 1988, "A model of tropical storm from temperature anomaly distribution", *Mausam*, **39**, 367-374.

Mandal, J. C., 1992, "A model of tropical storm boundary layer", *Mausam*, **43**, 259-268.

Miller, B. I., 1958, "The three dimensional wind distribution around a tropical cyclone," Nat. Hurr. Res. Proj. Report No. 15, 41.

Palmen, E. and Riehl, H., 1957, "Budget of angular momentum and energy in tropical cyclones," *J. Meteor.*, **14**, pp. 150-159

Palmen, E., 1958, "Vertical circulation and release of kinematic energy during the development of Hurricane Hazel into an extratropical storm," *Tellus*, **10**, pp. 1-23.

Riehl, H. and Malkus, J. S., 1961. "Some aspects of hurricane Daisy (1958)", *Tellus*, **13**, 181-213.

Riehl, H., 1963, "Some relations between wind thermal structure of steady state hurricanes", *J. Atmos. Sci.*, **20**, 276-287.

Rosenthal, S.L., 1969, Numerical experiments with a multi-level primitive equation model designed to simulate the development of tropical cyclones, Experiment I. ESSA, ERLTM-Nat. Hurr. Res. Lab. Tech. Memo. No. 82.

Shea, D. J. and Gray, W. M., 1973, "The hurricane's inner core region. I symmetric and asymmetric structure", *J. Atmos. Sci.*, **30**, 1544-1564.